Applied Catalysis B: Environmental 339 (2023) 123175

Contents lists available at ScienceDirect

Applied Catalysis B: Environmental

journal homepage: www.elsevier.com/locate/apcatb

Co-self-assembly of lignin and tannin: A novel catalyst support for hydrogenation of lignin-derived aldehydes

Xingjie Guo [a,b], Zhicheng Jiang [a,b,*], Ya Ma [a,b], Jiajun Fan [c], James H. Clark [c,**], Wenhua Zhang [a,b], Bi Shi [a,b]

[a] College of Biomass Science and Engineering, Sichuan University, Chengdu 610065, China
[b] National Engineering Research Center of Clean Technology in Leather Industry, Sichuan University, Chengdu 610065, China
[c] Circa Renewable Chemistry Institute, Green Chemistry Centre of Excellence, Department of Chemistry, University of York, York YO10 5DD, UK

ARTICLE INFO

Keywords:
Lignin
Tannin
Co-self-assembly
Pd catalyst
Vanillin hydrogenation

ABSTRACT

Co-self-assembly of lignin oligomers together with other structurally similar molecules can provide composite particles with functional properties for specific applications. Herein, tannin was co-self-assembled for the first time with lignin oligomers into novel lignin–tannin particles (L_xT_y), induced by a dual driven force with π–π stacking interaction and hydrogen bonds. Abundant *ortho*-phenolic hydroxyl groups of tannin cause the efficient adsorption and partial reduction of Pd^{2+} ions (36.7%) by L_xT_y (>99%) to obtain Pd/L_xT_y with highly dispersed Pd nanoparticles, thereby avoiding the need for surfactants or reducing agents. Aldehyde groups of lignin-derived aldehydes could preferentially interact with phenolic hydroxyl groups on the hydrophilic shell of Pd/L_xT_y. Then, mitigated active hydrogen atoms on the L_xT_y support during the hydrogen spillover process induced a H-shift to C of −C═O through a water bridge with low energy barrier and consequently selective hydrogenation to obtain lignin-derived alcohols at 30 °C.

1. Introduction

Lignin is a ubiquitous co-product in biorefineries but rarely offers a value stream other than through burning for energy. The growth of bio-based chemicals that is so widely sought must be based on more economically sound and low waste biorefineries: the more effective valorization of lignin is essential to that. Lignin is an aromatic natural polymer composed of three phenylpropane structural units connected by various aliphatic side chains containing C–C and C–O bonds [1,2]. Soluble lignin oligomers could be self-assembled into lignin nanoparticles with a benzene ring-stacked hydrophobic core and oxygen-containing functional groups of hydrophilic shell during the solvent-shifting process through weak intermolecular forces, including π–π interactions, hydrogen bonding, and electrostatic and hydrophobic forces [3,4]. It allows the direct utilization of lignin as mixed oligomers with different molecular sizes from the biomass degradation, without further complicated purification. Recently, drugs with similar chemical structures to lignin, such as doxorubicin and hydroxyl camptothecin, can co-self-assemble with lignin oligomers into composite nanoparticles to achieve drug delivery and sustained release [5,6]. Inspired by this concept, exploring other lignin-like molecules and investigating their co-self-assembly behavior and strength with lignin oligomers can provide a series of composite nanoparticles with functional properties for specific applications.

Monophenol-based chemicals are the building blocks from lignin degradation, and further oxidation/reduction will convert them into valuable chemicals [7–10]. Catalysts are necessary to enable selective oxidation/reduction paths and obtain target products with high selectivity due to diverse oxidizable/reducible functional groups on monophenol-based chemicals. For example, the catalytic hydro-conversion of vanillin (VAN), an important platform chemical from lignin degradation, involves hydrogenation of the aldehyde group to vanillyl alcohol (VAL), hydrodeoxygenation to 2-methoxy-4-methylphenol (MMP), and deep hydrogenation of the benzene ring to cycloalkanes [11,12]. Although VAL is an important chemical pharmaceutical intermediate and food additive, this reaction intermediate is difficult to obtain and subsequent reactions substantially reduce VAL selectivity. A series of Ni- and Pd-based catalysts were synthesized for VAN

* Corresponding author at: College of Biomass Science and Engineering, Sichuan University, Chengdu 610065, China.
** Corresponding author.
E-mail addresses: zhichengjiang@scu.edu.cn (Z. Jiang), james.clark@york.ac.uk (J.H. Clark).

https://doi.org/10.1016/j.apcatb.2023.123175
Received 30 June 2023; Received in revised form 4 August 2023; Accepted 11 August 2023
Available online 14 August 2023

hydrogenation, obtained a selectivity of < 80% for the VAL product, with the production of hydrodeoxygenated product MMP in the meantime [13,14]. An effective way to improve the selectivity of catalytic products is to control the interaction modes of the reaction substrate on the catalyst surface. Therefore, designing the catalyst structure and adjusting VAN adsorption through its aldehyde group on the catalyst surface can enhance VAL selectively.

Lignin nanoparticles are composed of a benzene ring-stacked core and a hydrophilic shell with diverse oxygen-containing groups [15]. Abundant hydrogen bonds may be generated between the shell of lignin nanoparticles and the aldehyde group of VAN, while the hydrophilic shell hinders π–π interactions between benzene rings in the core of lignin nanoparticles and the VAN molecule. These factors may cause the selective adsorption of VAN on lignin nanoparticles via the aldehyde group end of VAN, and thus lignin nanoparticles demonstrate potential as a catalyst support for VAN to VAL reaction. Lignin nanoparticles are the catalyst support that can anchor noble metal ions through electrostatic attraction and partly reduce metal ions [16,17]. However, additional heating was still required during the related process because of the inefficient adsorption and reduction capabilities of lignin. Therefore, tannin, a lignin-like substance existing in biomass, was extracted for co-self-assembly with lignin oligomers to prepare lignin–tannin composite particles with different ratios (L_xT_y, where x and y represent the weight proportions of initial lignin and tannin, respectively) [18]. The tannin constituent in L_xT_y could coordinately adsorb Pd^{2+} ions and reduce the metal ions due to the abundant *ortho*-phenolic hydroxyl groups [19,20]. Pd/L_xT_y was then employed for the catalytic hydrogenation of VAN to VAL in water under mild reaction conditions. The co-self-assembly behaviors of lignin and tannin as well as the selectively catalytic pathway were investigated through experiments and theoretical modeling.

2. Methods

2.1. Materials

Corncob residue and bayberry bark powder were obtained from local companies in China and washed and dried before the experiment. Tetrahydrofuran (THF), acetophenone, and K_2PdCl_4 were purchased from Aladdin Biochemical Technology Co., Ltd. (Shanghai, China). VAN and VAL were acquired from J&K Scientific Co., Ltd. (Beijing, China). Syringaldehyde, MMP, syringyl alcohol, p-hydroxybenzaldehyde, and p-hydroxybenzyl alcohol were bought from Sigma–Aldrich Co., Ltd. (Shanghai, China). All the chemicals were used as received without further purification.

2.2. Extraction of lignin and tannin

Our previous work demonstrated that H_2O-THF (3:7, vol:vol) co-solvent was used for the solvothermal extraction of lignin and tannin from corncob residue and bayberry bark, respectively [21]. The extraction of lignin was carried out in a sealed Parr autoclave with a mechanical stirrer. A lignin oligomer-rich liquid was separated from the reaction solid residue after reaction at 200 °C for 1 h. Similarly, the extraction of tannin was carried out in a three-necked flask with mechanical stirring at 60 °C for 2 h. The degradation treatment was performed to convert the insoluble lignin in the corncob residue into lignin oligomers soluble in organic solvents, thus facilitating the subsequent preparation of nanoparticles via self-assembly. The concentrations of lignin oligomers and tannin in the two liquids were measured at 16.79 and 19.55 mg/mL, respectively.

2.3. Synthesis of Pd/L_xT_y

The synthesis of Pd/L_xT_y comprises the following steps: i) preparation of L_xT_y particles and ii) stabilization of Pd on L_xT_y particles. A series of L_xT_y particles with different lignin/tannin initial mass ratios (4:0, 3:1, 2:2, 1:3, and 0:4) were synthesized using the ultrasonic-assisted solvent shifting method. Solvent shifting method is a common method to prepare lignin nanoparticles, and its mechanism is to reduce the solubility of lignin and tannin by changing the solvent environment, which leads to the formation of nanoparticles driven by hydrophobic interactions, π-π stacking, hydrogen bond, etc. First, according to the designing lignin/tannin ratio, the lignin and tannin liquids with a total solid content of 500 mg were added to a beaker, which was placed in an ultrasound sink. The total concentration was adjusted to 5 mg/mL with fresh H_2O-THF co-solvent (3:7, vol:vol). Second, distilled water was added into the beaker dropwise at a flow rate of 5 mL/min until H_2O occupied 90 vol% of the final liquid. Finally, colloidal solutions containing L_xT_y particles were centrifuged at 10,000 rpm for 10 min, washed three times with distilled water, and freeze-dried to obtain L_xT_y particles (L_4T_0, L_3T_1, L_2T_2, L_1T_3, and L_0T_4). Meanwhile, K_2PdCl_4 solution was added to the L_xT_y particle-containing solution and then stirred at room temperature for 24 h according to the designing Pd loading content. Finally, colloidal solutions of Pd/L_xT_y particles were centrifuged at 10,000 rpm for 10 min, washed three times with distilled water, and freeze-dried to obtain Pd/L_xT_y particles.

2.4. Characterization of solid samples

L_xT_y particles were redissolved in deuterated chloroform and pyridine and detected via nuclear magnetic resonance spectroscopy (Bruker AV II-600 MHz) for ^{31}P NMR analysis [22,23]. Fluorescence properties of L_xT_y particles were examined using confocal laser microscopy (Leica STELLARIS) at excitation wavelengths of 488 and 594 nm. Water contact angle of L_xT_y particles was measured with a drop shape analyzer (DSA30S, KRÜSS). The adsorption of Pd on L_xT_y particles was obtained by quantitatively measuring the Pd concentration in the post-adsorption liquid using inductively coupled plasma atomic emission spectroscopy (ICP-AES, 5100SVDV, Agilent Technologies). Zeta potential measurements of L_xT_y and Pd/L_xT_y particles in the aqueous solution were performed with a particle size analyzer (NanoBrook Omni, Brook Haven). The X-ray diffraction (XRD) patterns of Pd/L_xT_y particles were obtained from an X-ray diffractometer (Rigaku Ultima IV) with Cu–Kα as the X-ray source (40 KV, 40 mA). X-ray photoelectron spectroscopy (XPS) patterns of Pd/L_xT_y particles were measured with an X-ray photoelectron spectrometer (ESCALAB 250Xi, Thermo Fisher) with Al–Kα as the X-ray source. The morphology of L_xT_y particles and the distribution of Pd particles loaded on the surface of L_xT_y particles were detected via scanning (SEM, JSM-7500 F, JEOL) and transmission (TEM, Talos F200S G2, Thermo Fisher) electron microscopies. The reaction solution was freeze-dried and redissolved in D_2O for ^1H NMR analysis (Bruker AV II-400 MHz).

2.5. Catalytic hydrogenation of vanillin and product analysis

Catalytic hydrogenation experiments of VAN were carried out in a stainless-steel autoclave reactor with a mechanical stirrer (50 mL, Shijisenlang, China). VAN (2 mmol), 3% Pd/L_xT_y (20 mg), and distilled water (20 mL) were added into the reactor for a typical hydrogenation experiment. The air in the reactor was replaced with H_2 5 times and H_2 pressure was maintained at 1 MPa after the reactor was sealed. The reactor was then heated to 50 °C and then maintained for 1 h with mechanical stirring at a speed of 500 rpm. The reactor was rapidly cooled and the catalyst was separated from the reaction solution via filtration when the reaction was completed.

Before detection, the reaction solution was treated by rotary evaporation to remove water solvent, and then the products were redissolved in ethanol containing acetophenone as the internal standard. The reaction solution was first detected using gas chromatography–mass spectrometry (GC–MS, Agilent 6890 N) to determine the reaction products. The reaction solution was then quantitatively analyzed via gas

chromatography (GC, Agilent 8890) with a flame ionization detector to calculate the VAN conversion and VAL selectivity as follows:

$$\text{Conversion}\ (\%) = (n_{initial} - n_{remained}) / n_{initial} \times 100\% \quad (1)$$

$$\text{Selectivity}\ (\%) = n_{product} / (n_{initial} - n_{remained}) \times 100\% \quad (2)$$

where $n_{initial}$ represents the moles of the initial VAN used in the reaction, $n_{remained}$ is the moles of the remaining VAN after the reaction, and $n_{product}$ is the moles of each product generated in the reaction.

2.6. Calculation of turnover frequency and apparent activation energy

Metal dispersion of Pd (D_{Pd}) and turnover frequency (TOF) can be expressed as follows:

$$D_{Pd} = (N_S / N_T) \times 100\% \quad (3)$$

$$TOF = (n_{initial} - n_{remained}) / (n_{Pd} \times D_{Pd} \times t) \quad (4)$$

where N_S is the number of surface Pd atoms, N_T is the total number of Pd atoms in a Pd particle by using a mathematical model for cuboctahedral particles [24], n_{Pd} accounts for the moles of the Pd on the Pd/L_xT_y catalyst, and t is the reaction time (10 min).

Chemical kinetics and apparent activation energy (E_a) for catalytic hydrogenation of VAN to VAL could be expressed as follows:

$$C_0 - C_t = C_0 (1 - e^{-kt}) \quad (5)$$

$$\ln k = -E_a / RT + \ln A \quad (6)$$

where C_0 is the initial concentration of VAN, C_t accounts for the concentration of VAN at 10 min, k is the kinetic constant, R is the gas constant, T is the reaction temperature, and A is the pre-exponential factor.

2.7. Hydrogen spillover experiments

Hydrogen spillover experiments were carried out in a quartz tube. Pd/L_2T_2 (3%, 10 mg) and WO_3 (1 g) were mixed into a quartz tube and stored in H_2 atmosphere (flow rate of 20 mL/min) at room temperature for 10 min in a typical experiment. Meanwhile, a control hydrogen spillover experiment was conducted using pure WO_3 and mixed L_2T_2-WO_3.

2.8. Comparison of 3% Pd/SiO_2 and 3% Pd/SiO_2-L_2T_2

The synthesis of 3% Pd/SiO_2 was divided into the following steps: i) calcination of SiO_2 in a tube furnace under N_2 atmosphere at 800 °C for 2 h (heating rate of 5 °C/min); ii) K_2PdCl_4 solution was added to the SiO_2 colloidal solution (1 mg/mL) and stirred for 24 h; iii) ascorbic acid was added and stirred for 2 h to reduce Pd; and iv) the resulting solution was centrifuged, washed, and dried to obtain 3% Pd/SiO_2. The 3% Pd/SiO_2-L_2T_2 was obtained by physically compressing 3% Pd/SiO_2 with additional L_2T_2 into compact sheets. A low speed of 50 rpm was used when comparing the catalytic VAN hydrogenation of these two catalysts to prevent the collapse of catalyst sheets. Hydrogen spillover experiments of 3% Pd/SiO_2 and 3% Pd/SiO_2-L_2T_2 used the same conditions as the previous hydrogen spillover experiments.

2.9. Adsorption experiments

Adsorption experiments were carried out for the efficient hydrogenation of VAN to reveal the catalytic mechanism of Pd/L_xT_y. First, 100 mg of VAN or VAL was dissolved in 20 mL of distilled water and then 20 mg of Pd/L_xT_y catalyst was added to the solution. Solid and liquid parts were rapidly separated by centrifugation after stirring for 30 min. The solid was dried and detected via Fourier transform infrared spectrometer (FT-IR, Nicolet iS50, Thermo Fisher), and the liquid was measured using ultraviolet spectroscopy (UV, 1800 BPC spectrophotometry) to determine the concentration of the remaining VAN or VAL.

2.10. Molecular dynamics simulation

Molecular dynamics simulation was performed on GROMACS 2020.6 to investigate the aggregation behaviors of lignin–lignin, tannin–tannin, and lignin–tannin during the self-assembly process as well as the adsorption mode of VAN on the catalyst support. The self-assembly process was simulated in the H_2O-THF (9:1, vol:vol) co-solvent. A lignin-derived dimer (two guaiacyl groups joined by a β-O-4 linkage) was used as the model compound of lignin, while gallocatechin was utilized as the model compound of tannin. CHARMM general force field (CGenFF) parameters were applied to the molecules of lignin, tannin, THF, and VAN, while molecules of water were described through the TIP3P model [25,26]. Trajectory data obtained in each simulated system were analyzed using visual molecular dynamics (VMD) and GROMACS. Each simulated system was filled with model molecules in a simulation box (10 nm × 10 nm × 10 nm) under a periodic boundary condition. In addition, steepest-descent energy minimization was performed for each system to remove accidental overlaps. Molecular dynamics simulations were conducted at room temperature for 100 ns, and equilibrium was analyzed in the last 50 ns.

2.11. Quantum chemical calculations

Full geometry optimizations were performed in the aqueous solution using the M062X method [27], with the def2tzvp basis set [28] M062X/def2tzvp, to locate all stationary points. The self-consistent reaction field method based on the universal solvation model SMD was adopted to evaluate the effect of the solvent [29]. Gibbs free energy of formation (ΔG) is relative to the initial reactants, including ZPE correction obtained at the M062X/def2tzvp level, unless otherwise specified. All geometry calculations were run with the Gaussian 09 program.

3. Results and discussion

3.1. Co-self-assembly behaviors of lignin and tannin

Five kinds of L_xT_y particles with different initial mass ratios of lignin and tannin and a total input of 500 mg of each sample were prepared using the solvent shifting method (Fig. 1a). The mass of the obtained L_4T_0 was 362 mg, which is nearly twice that of L_0T_4 (186 mg), thereby indicating the better self-assembly ability of lignin than that of tannin. This finding might be because the aliphatic connections between the benzene rings of lignin could easily rotate; thus, the adjustable angle between the benzene rings in two lignin-based molecules benefited from their π–π interaction [30,31]. The theoretical yield of L_xT_y was calculated on the basis of the yields from independently self-assembled lignin (L_4T_0) and tannin (L_0T_4) when lignin and tannin were mixed and self-assembled, as shown in Fig. 1a. Notably, higher actual yields than theoretical yields of L_xT_y revealed that lignin and tannin might self-assemble together to form L_xT_y particles in a new co-self-assembly manner rather than a simple mixture of lignin and tannin particles. Physical and chemical properties of L_xT_y particles were analyzed using ^{31}P NMR, water contact angle, and confocal laser fluorescence microscopy (Fig. 1b–d). Among the L_xT_y particles, L_4T_0 demonstrated the highest content of aliphatic hydroxyl groups while L_0T_4 showed the highest content of phenolic hydroxyl groups likely due to the structural features of lignin and tannin. The majority of phenolic hydroxyl groups on phenol-based units of lignin are hidden by the condensation, and abundant alcoholic hydroxyl groups exist on the side chain [32]. Meanwhile, tannin is composed of phenolic hydroxyl-rich catechin units connected by C–C bonds [33,34]. The increasing tannin content in L_xT_y particles with high total hydroxyl content also resulted in high

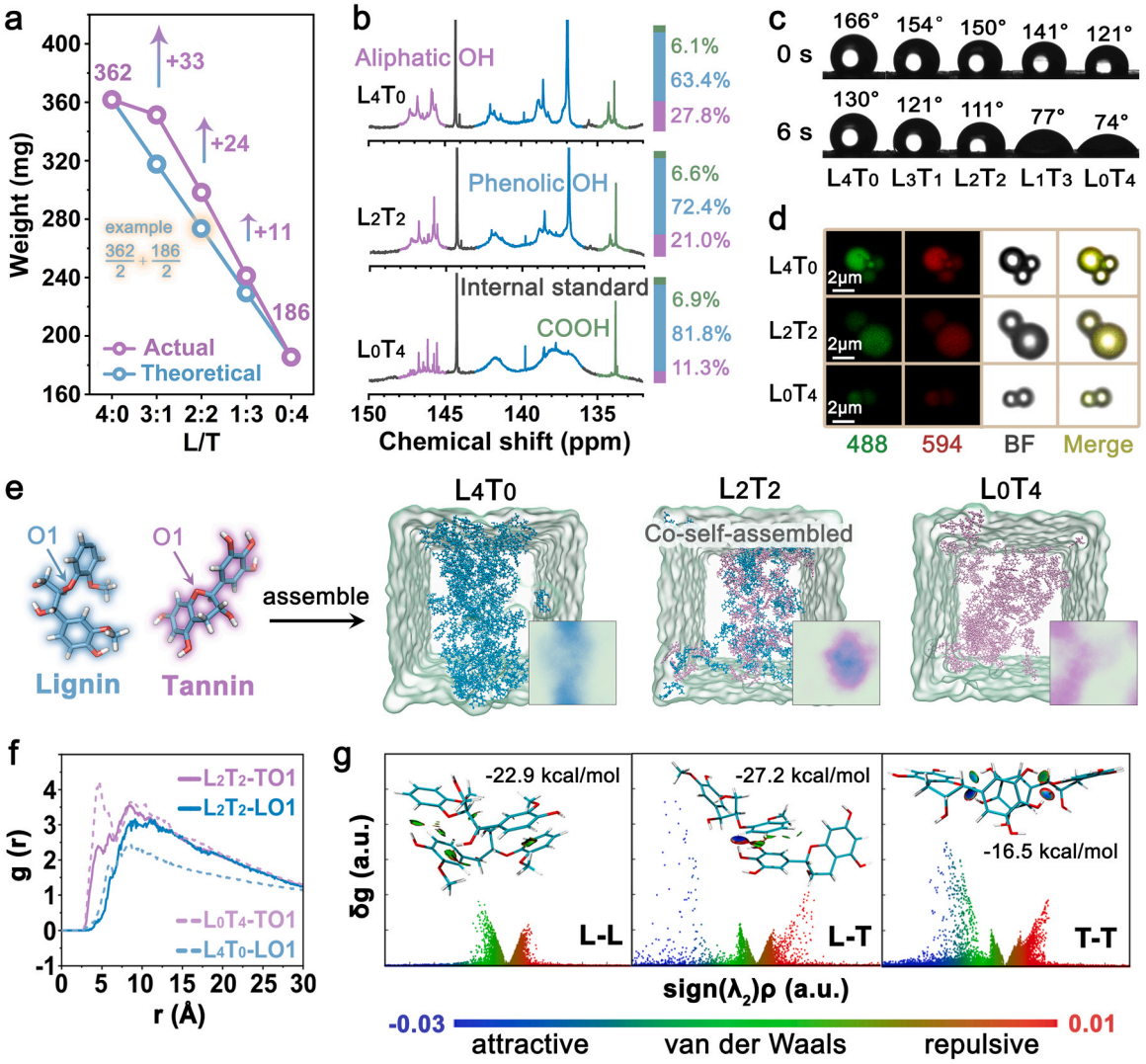

Fig. 1. Main properties and molecular dynamics simulation of L_xT_y particles. (a, Yield of L_xT_y particles. b, ^{31}P NMR spectrums of the redissolved L_xT_y particles. c, Water contact angles images of L_xT_y particles. d, Confocal microscopy images of L_xT_y particles. e, Lignin-derived and tannin-derived model compounds, and the molecular dynamics simulations. f, Radial distribution function plot of O1 in different systems. g, Interactions of the lignin-derived and tannin-derived model compounds.).

hydrophilic property [35]. These results revealed that both lignin and tannin participate in the co-self-assembling process for L_xT_y particles. From fluorescence microscope under an excitation of 488 and 594 nm, the brightness of L_4T_0 particles was clearly stronger than that of L_0T_4 particles. Note that the brightness of L_2T_2 particles is similar, with a level between that of L_4T_0 and L_0T_4 particles instead of a mixture of bright and dark particles. This finding further verified the co-self-assembly of lignin and tannin to generate L_xT_y particles.

Molecular dynamics simulations were performed to observe the self-assembly behavior of lignin and tannin visually. Lignin and tannin model compounds with different ratios (4:0, 2:2, and 0:4) after reaching the steady state in the H_2O-THF co-solvent are presented in Fig. 1e. All three cubes of molecules, especially lignin and tannin molecules in L_2T_2, showed tendencies to aggregate together without individual lignin and tannin clusters. Meanwhile, radical distribution function (RDF) was introduced to evaluate the distribution of reference atoms in lignin and tannin molecules with a certain distance to the corresponding atom in each finding molecule, where r represents the radius between the reference and finding atoms and $g(r)$ represents the relative density of finding atoms [36,37]. As shown in Fig. 1f, the maximum $g(r)$ value of the lignin molecules in the L_4T_0 system appeared at $r = 8.1$ Å, while it increased to r = 9.2 Å in the L_2T_2 system. Similarly, the maximum $g(r)$ value of tannin molecules appeared at $r = 4.7$ Å in the L_0T_4 system and $r = 8.4$ Å in the L_2T_2 system. Distances of both lignin–lignin and tannin–tannin in the mixed system (L_2T_2) are longer than those in pure systems (L_4T_0 and L_4T_0). This finding further confirmed that lignin and tannin molecules self-assembled with each other.

The interaction behavior and strength during self-assembly were investigated using the aforementioned lignin and tannin model compounds via DFT analysis. As shown in Fig. 1g, interaction energies of lignin–lignin (L–L), lignin–tannin (L–T), and tannin–tannin (T–T) were calculated. These interactions were classified using an independent gradient model, in which blue is for weak interactions (hydrogen bonds, halogen bonds, ionic bonds), green is for Van der Waals interactions, and red is for repulsion interactions (steric effect on rings and cages). Consistent with the experimental results, L–L exhibited a stronger interaction with − 22.9 kcal/mol of interaction energy than T–T (−16.5 kcal/mol) and interaction forces of these two self-assembly behaviors were different. The L–L interaction was dominantly driven by the π–π stacking interaction (green area), while hydrogen bonds (blue area) were the main interaction force for T–T because many phenolic hydroxyl groups of tannin would form multi-point hydrogen bonds.

Notably, a dual driven force with π–π stacking interaction and hydrogen bonds resulted in the strongest L–T interaction with − 27.2 kcal/mol of interaction energy. This finding indicated an efficient co-self-assembly between lignin oligomers and tannin.

3.2. Composition effect of lignin/tannin ratio

Co-self-assembled L_xT_y composite particles were used as the catalyst support to load and reduce Pd^{2+} due to abundant oxygen-containing groups (hydroxyl and carboxyl groups) in lignin and *ortho*-phenolic hydroxyls in tannin [38,39]. As shown in Fig. 2a, 93.7% of Pd^{2+} was stabilized on L_4T_0 particles and the stabilization efficiency improved with the increase of tannin content in the L_xT_y support due to the stronger adsorption ability of tannin through the coordination between *ortho*-phenolic hydroxyls and Pd^{2+} than that of lignin through electrostatic adsorption [40,41]. The high content of phenolic hydroxyls in tannin also led to the low zeta potential of tannin-dominated L_xT_y particles (Fig. 2b). The following Pd^{2+} coordination would then occupy the negatively charged groups on particles to increase the zeta potential. However, the poor self-assembly of L_0T_4 particles might lead to part of the oxygen-containing groups did not follow the outward orientation during the self-assembly process, resulting in a decrease in the absolute value of the zeta potential of L_0T_4 compared with that of L_1T_3.

A series of Pd/L_xT_y materials were characterized via XRD and XPS analyses to reveal the crystalline structures and valence state distributions of Pd. Although nearly 3 wt% of Pd stabilized on the L_xT_y support, the diffraction peak of Pd species was unclear (Fig. 2c) likely due to the high dispersion of Pd species on L_xT_y. Among the five Pd/L_xT_y catalysts, the content of Pd^0 increased from 9.8% to 36.7% depending on the increasing tannin ratio in the L_xT_y support (Fig. 2d). However, the signal-to-noise ratio and the surface Pd content from XPS analysis decreased with increasing tannin content. It might be attributed to the poor self-assembly of the tannin-dominant particles, where part of the oxygen-containing groups were oriented towards the interior of the particles. As a result, the palladium ions adsorbed on the interior of the L_xT_y particles were beyond the detectable range of the XPS instrument. The comparison of the XPS O1s spectra of L_2T_2 and Pd/L_2T_2 (Fig. S1) revealed that the O═C content increased from 20.7% to 33.8% after Pd loading due to the oxidation of the tannin phenolic hydroxyl group to a quinone structure. Therefore, *ortho*-phenolic hydroxyls in tannin captured Pd^{2+}, reduced Pd^{2+} to Pd^0, and self-oxidized to quinones (Figs. 2e and S2) [42].

SEM and TEM were employed to examine the effect of lignin and tannin contents on the morphology of Pd/L_xT_y catalysts and observe the microstructures of the L_xT_y support and Pd distribution (Fig. 3). The five L_xT_y supports with different lignin/tannin ratios were uniform spheres with a mean particle size ranging from 0.9 μm to 2.2 μm. Particle sizes of L_4T_0 or L_0T_4 were intensively distributed, while those of the co-self-assembled L_xT_y (L_3T_1, L_2T_2, and L_1T_3) were distributed in a wide range because the uniform interaction force among the molecules with similar structures lead to a uniform size of assembled particles and vice versa [43]. Increasing the tannin content resulted in a rough surface of L_xT_y particles and a slight decrease in particle size due to the poor self-assembly ability of tannin and its low molecular weight (Fig. S3). Pd particles were evenly dispersed on the surface of L_xT_y particles after Pd loading and the highly distributed C, O, and Pd signals in EDX-mapping images also confirmed the homogeneous dispersion. The average Pd particle size on the pure lignin L_4T_0 was only 3.2 nm, which increased on tannin-participated L_xT_y particles. The higher adsorption ratio of Pd^{2+} and strong reduction ability of tannin caused the accumulation of Pd species into large particles [44]. The Pd particle size of Pd/L_0T_4 was smaller than that of Pd/L_1T_3, probably ascribed to that smaller particle size of L_0T_4 possessed larger specific surface area, which promoted the dispersion of palladium ions and inhibited the aggregation of Pd particles. The high-resolution TEM image revealed that the lattice spacing distances on Pd particles are 0.225 nm, which corresponds to the (111) crystal plane of Pd [45].

3.3. Pd/L_xT_y catalyzed VAN hydrogenation

The catalytic performance of the prepared Pd/L_xT_y particles on VAN hydrogenation was evaluated in H_2O at 50 °C (Fig. 4a–c). Only VAL generated a selectivity of nearly 100% while the hydrodeoxygenated product of MMP, deep hydrogenation of benzene ring and condensation of VAL were undetected in each hydrogenation process, which could be confirmed by the NMR analysis of the reaction products (Fig. S4). The

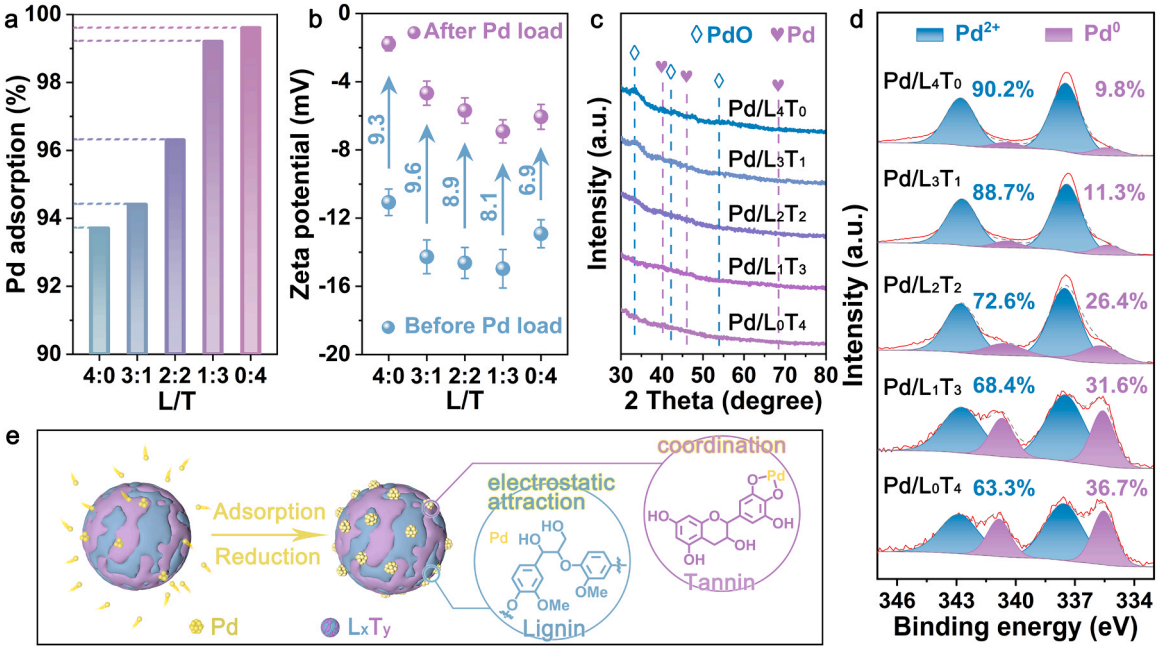

Fig. 2. Structural characterizations of the Pd/L_xT_y catalysts. (a, Pd^{2+} absorption on L_xT_y particles. b, Zeta potential values of L_xT_y particles and 3% Pd/L_xT_y particles. c, XRD patterns of 3% Pd/L_xT_y particles. d, XPS spectra of 3% Pd/L_xT_y particles. e, Schematic diagram of 3% Pd/L_xT_y particles preparation.).

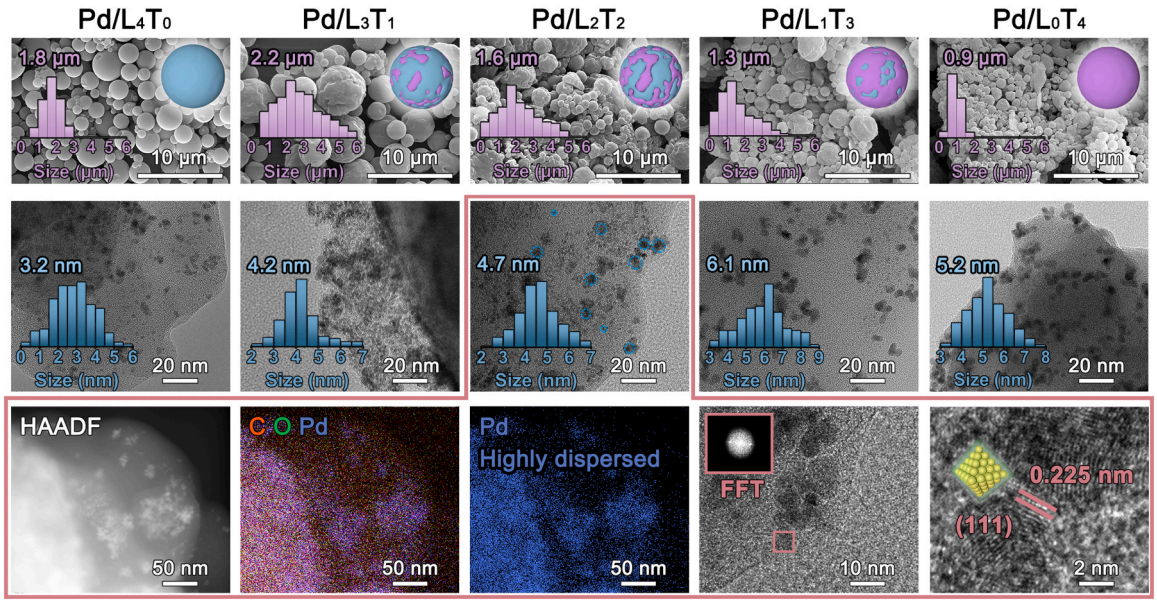

Fig. 3. SEM and TEM images of L_xT_y particles and 3% Pd/L_xT_y catalysts. (1st row, SEM images of L_xT_y particles. 2nd row, TEM images of 3% Pd/L_xT_y catalysts. 3rd row, EDX-mapping and HRTEM images of 3% Pd/L_2T_2.).

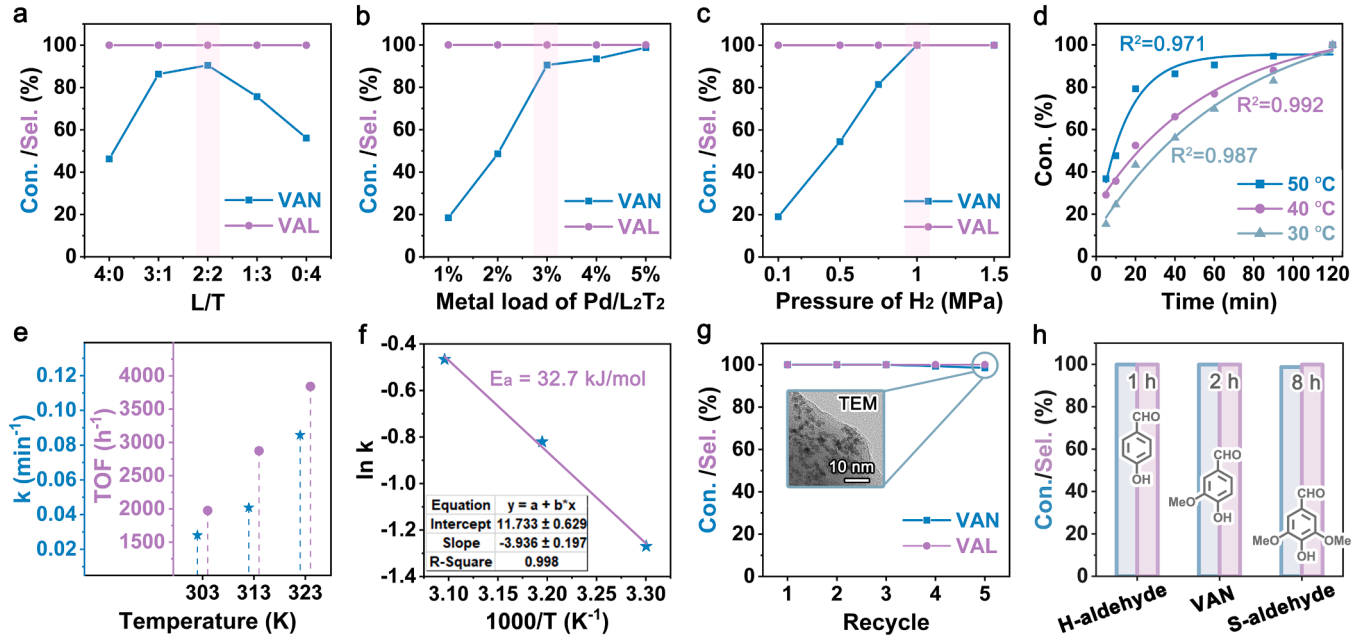

Fig. 4. Catalytic Hydrogenation of VAN. (a, Different L_xT_y particles as supports. b, Loading amount of Pd. c, Pressure of H_2. d, Kinetics of 3% Pd/L_2T_2 catalysis. e, *k* and TOF of 3% Pd/L_2T_2 catalysis for 10 min f, E_a of 3% Pd/L_2T_2 catalysis. g, Stability of 3% Pd/L_2T_2 catalyst. h, 3% Pd/L_2T_2 catalyzed hydrogenations of different lignin-derived aldehydes.).

high selectivity probably ascribed to the mild reaction conditions and the absence of strong acidic sites in the support. Specifically, the VAN conversion reached 90.3% when using the 3% Pd/L_2T_2 catalyst prepared from co-self-assembly of lignin and tannin and below 60% when catalyzed by 3% Pd/L_4T_0 or 3% Pd/L_0T_4. In addition, the TOF value of 3% Pd/L_2T_2 was the highest among the five catalysts (Fig. S5). The low adsorption and reduction degree of Pd^{2+} on lignin-dominated particles as well as the aggregation of Pd on tannin-dominated particles caused inefficient VAN hydrogenation. Besides, high Pd loading on L_2T_2, initial H_2 pressure and Pd loading (Figs. S6 and S7) could promote the VAN hydrogenation and result in formation of VAL; meanwhile, VAN conversion reached a maximum of 99.9%.

The kinetics of hydrogenation conversion of VAN was systematically investigated in the temperature range of 30–50 °C (Fig. 4d). Fig. 4e illustrates the reaction rate (*k*) and turnover frequency (TOF) of the 3% Pd/L_2T_2 catalyst at different temperatures with a reaction time of 10 min. The TOF of this catalyst increased with the increase of temperature at 1975.4 h^{-1} at 30 °C, 2873.0 h^{-1} at 40 °C, and 3840.1 h^{-1} at 50 °C. The apparent activation energy (E_a) of our catalytic process was 32.7 kJ/mol (Fig. 4f), thereby demonstrating the high efficiency of our catalyst [46]. More than 99.9% of VAN conversion and VAL selectivity could be achieved at 30 °C within 120 min in the presence of 1 MPa H_2 after optimizing the reaction conditions. According to the recycling test of the 3% Pd/L_2T_2 catalyst, the catalytic efficiency and the catalyst

properties showed a negligible change during five recycle experiments (Figs. 4g and S8), which revealed the high stability of Pd/L_2T_2 and its potential industrial application. Meanwhile, the carbon balance was close to 100% in all VAN hydrogenation reactions in this work. The high carbon balance might be attributed to mild reaction conditions that inhibit further hydrodeoxygenation or polymerization of the produced VAL [47].

In addition to vanillin (G-aldehyde), p-hydroxybenzaldehyde (H-aldehyde) and syringaldehyde (S-aldehyde) were adopted as starting materials to evaluate the catalytic hydrogenation potential for lignin-based aldehydes (Fig. 4h). Similarly, selective hydrogenation of aldehyde groups to hydroxyl groups occurred in the absence of hydrodeoxygenation and benzene ring hydrogenation. However, different reaction times were required to achieve the high conversion of lignin-based aldehydes to related alcohols, where the hydrogenation reaction capabilities of our catalyst for the three lignin-based aldehydes decreased in the following order: p-hydroxybenzaldehyde > vanillin > syringaldehyde. Slow hydrogenation of G-aldehyde and S-aldehyde might be attributed to the electron-rich features of these two molecules from the substituted methoxyl groups on the benzene ring.

3.4. Proposed catalytic reaction path

For the catalytic hydrogenation reaction, behaviors of hydrogen activation and migration on the support surface would significantly affect the catalytic performance. The hydrogen spillover phenomenon of the Pd/L_2T_2 catalyst was observed (Fig. 5a), and yellow WO_3 reacted with active hydrogen atoms on the surface of the catalyst support to form dark blue H_x·WO_3 [48,49]. This finding verified that hydrogen atoms activated by the Pd species could migrate to the surface of the L_xT_y support to ensure that the support also becomes active for catalysis [50]. Comparing the XPS O1s spectra of Pd/L_2T_2 (Fig. S1), the reduced O═C content and the increased O−C content after H_2 treatment revealed that the hydrogen spillover on the support surface occurred through the structural transformation of quinone into phenolic hydroxyl group. Therefore, the catalytic hydrogenation of VAN could happen both on the Pd species and the L_xT_y support.

VAN hydrogenation and hydrogen spillover experiments were compared using 3% Pd/SiO_2 and compressed 3% Pd/SiO_2 with L_2T_2 (no catalytic ability) to ascertain the preferential hydrogenation site (Fig. 5b). The conversion of VAN was catalyzed by less than 10% with 3% Pd/SiO_2 but nearly twice that when using the 3% Pd/SiO_2-L_2T_2 catalyst. VAN hydrogenation could only occur on Pd species given that SiO_2 is an inert support for hydrogen spillover [51]. Thus, the poor VAN conversion catalyzed by 3% Pd/SiO_2 demonstrated ineffective VAN hydrogenation on the Pd species. Notably, the physically compressed 3% Pd/SiO_2 with L_2T_2 obviously promoted the VAN conversion. The darkened WO_3 with the 3% Pd/SiO_2-L_2T_2 catalyst during the hydrogen spillover experiments indicated the migration of Pd/SiO_2-activated hydrogen atoms onto the L_2T_2 support surface, and further catalysis of the VAN hydrogenation happened directly on the L_2T_2 support.

Therefore, adsorption behaviors of the VAN substrate and the VAL product on the L_xT_y support surface played a decisive role for the reaction rate and the hydrogenation selectivity [52]. Pd/L_2T_2 exhibited a significantly higher adsorption rate of VAN than that of VAL (Fig. 5c and d). Hence, effective VAN conversion was achieved and VAL was rapidly released from the catalyst surface after generation to avoid further hydrogenation. The adsorption manner of VAN on L_2T_2 particles was investigated using molecular dynamics simulation (Fig. 5e). The L_2T_2 particle surface rich in oxygen-containing groups could easily adsorb

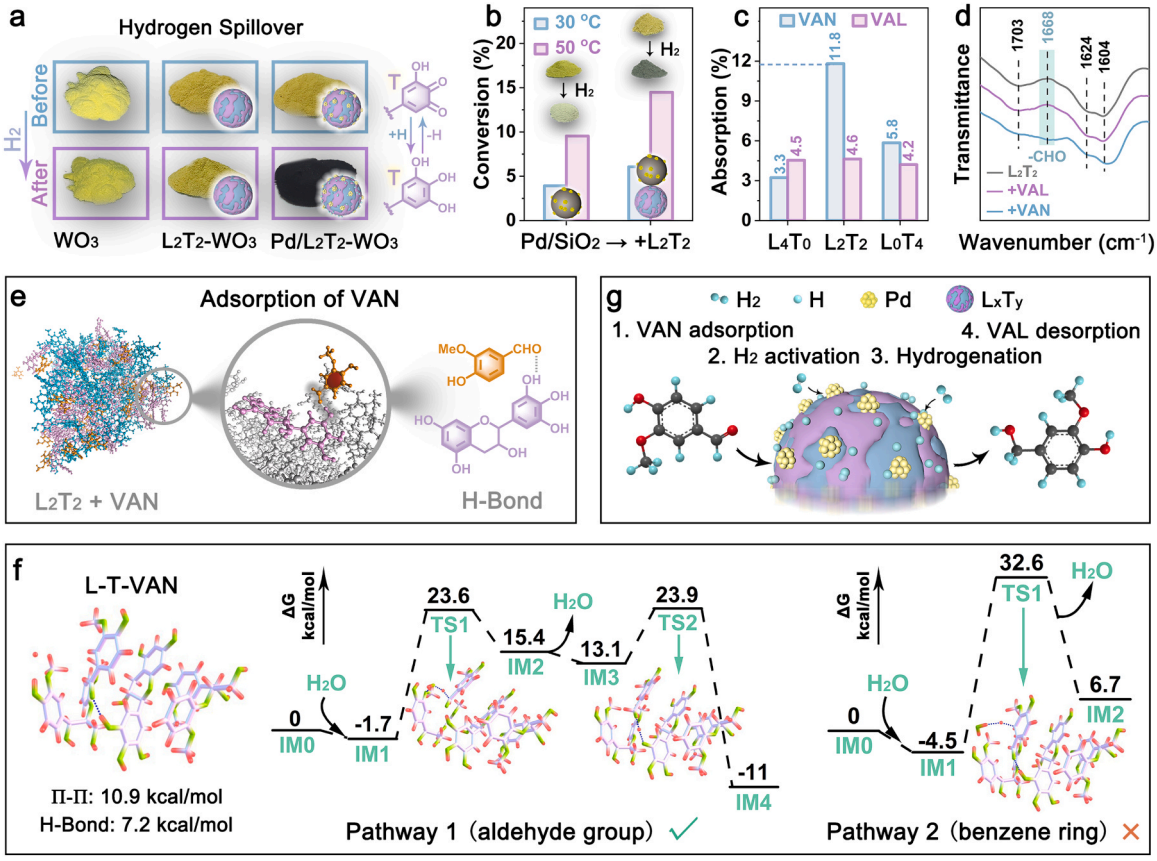

Fig. 5. Proposed catalytic reaction path. (a, Hydrogen spillover experiment. b, VAN conversion and hydrogen spillover of 3% Pd/SiO_2 and 3% Pd/SiO_2-L_2T_2. c, The adsorption performance of VAN and VAL on L_xT_y. d, FT-IR spectra of the L_2T_2 and the post-adsorption samples. e, Simulation of VAN adsorption on L_2T_2. f, Quantum chemical calculations of the two hydrogenation pathways. g, Proposed catalytic reaction mechanism.).

VAN with their hydrophilic shell and hydrophobic core. Therefore, hydrogen bonding interaction occurred between the phenolic hydroxyl group of tannin and the aldehyde group of VAN, thereby tilting the aromatic ring of VAN away from the surface and consequently altering the noble metal-favoring planar configurations [53].

The hydrogenation reaction path on the L_xT_y support was investigated on the basis of the adsorption site via quantum chemical calculations to understand hydrogenation selectivity further (Fig. 5f). At the beginning of the reaction, a stable complex was generated by the consisting of lignin and tannin, due to the hydrogen bonding and the π–π interactions, with energies of 7.2 and 10.9 kcal/mol, respectively. In this regard, the two potential hydrogenation pathways are aldehyde group (Pathway 1) and benzene ring (Pathway 2) hydrogenation. It was calculated that the former model was realized by the H-shift to C of −C═O through a water bridge with an energy barrier of 25.3 kcal/mol. By contrast, the energy barrier for the H-shift direct to the benzene ring was 37.1 kcal/mol, which was higher than that for the aldehyde group hydrogenation. Therefore, VAL was selectively produced because aldehyde group hydrogenation was prioritized over benzene ring hydrogenation in this catalytic system.

4. Conclusions

A series of L_xT_y particles were prepared for the first time as catalyst supports by co-self-assembly via the solvent-shifting method to maximize the structural features of biomass of strong self-assembly ability of lignin and in situ reduction ability of tannin. Although high tannin content in L_xT_y particles could adsorb and reduce additional Pd^{2+} ions, the Pd species would aggregate into large Pd particles. Pd/L_xT_y particles were then applied for the catalytic hydrogenation of VAN. 3% Pd/L_2T_2 selectively catalyzed hydrogenation of the aldehyde group of VAN into the hydroxymethyl group, wherein both VAN conversion and VAL selectivity were greater than 99.9% in water solvent under 1 MPa of H_2 at 30 °C for 2 h. A low E_a (32.7 kJ/mol) and a high TOF (1975.4 h^{-1}) at 30 °C also confirmed the excellent catalytic ability. The adsorption of the aldehyde group of VAN on the phenolic hydroxyl group on the catalyst support determined the high selectivity to obtain VAL. Our work fully utilized lignin with multiple molecular scales ranging from oligomers as catalyst support to small molecule products to help develop a whole biomass-derived chemical industrial process that can complement existing and future polysaccharide-focused biorefineries.

CRediT authorship contribution statement

Xingjie Guo: Investigation, Methodology, Writing – original draft, Data curation. **Zhicheng Jiang**: Investigation, Funding acquisition, Supervision, Writing – review & editing. **Ya Ma**: Methodology, Software. **Jiajun Fan**: Investigation, Methodology. **James H. Clark**: Investigation, Writing – review & editing. **Wenhua Zhang**: Investigation, Supervision, Resources. **Bi Shi**: Supervision, Resources.

Declaration of Competing Interest

The authors declare that they have no known competing financial interests or personal relationships that could have appeared to influence the work reported in this paper.

Data availability

Data will be made available on request.

Acknowledgments

This work is financially supported by the National Natural Science Foundation of China (22078211). We appreciate Hui Wang from the Analytical & Testing Center of Sichuan University for helping with the SEM characterization. We also thank Dr. Xiu He and Dr. Ying Song at College of Biomass Science and Engineering, Sichuan University, for the experimental assistance.

Appendix A. Supporting information

Supplementary data associated with this article can be found in the online version at doi:10.1016/j.apcatb.2023.123175.

References

[1] M. Wang, F. Wang, Catalytic scissoring of lignin into aryl monomers, Adv. Mater. 31 (2019) 1901866.
[2] B. Wang, Y. Sun, R. Sun, Fractionational and structural characterization of lignin and its modification as biosorbents for efficient removal of chromium from wastewater: a review, J. Leather Sci. Eng. 1 (2019), 5.
[3] Z. Jiang, Y. Ma, X. Guo, J. Remón, D.C.W. Tsang, C. Hu, B. Shi, Sustainable production of lignin micro-/nano-particles (LMNPs) from biomass: influence of the type of biomass on their self-assembly capability and physicochemical properties, J. Hazard. Mater. 403 (2021), 123701.
[4] H. Sun, G. Wang, J. Ge, N. Wei, W. Sui, Z. Chen, H. Jia, A.M. Parvez, C. Si, Reduction of lignin heterogeneity for improved catalytic performance of lignin nanosphere supported Pd nanoparticles, Ind. Crop. Prod. 180 (2022), 114685.
[5] Y. Zhou, Y. Han, G. Li, F. Xiong, F. Chu, Lignin-based fluorescence hollow nanoparticles: their preparation, characterization, and encapsulation properties for doxorubicin, Int. J. Biol. Macromol. 165 (2020) 2136–2142.
[6] K. Liu, D. Zheng, H. Lei, J. Liu, J. Lei, L. Wang, X. Ma, Development of novel lignin-based targeted polymeric nanoparticle platform for efficient delivery of anticancer drugs, ACS Biomater. Sci. Eng. 4 (2018) 1730–1737.
[7] J. Yan, R. Liu, Z. Li, P. Fu, P. Geng, W. Yi, Gas-phase catalytic hydrodeoxygenation of phenolic compounds derived from lignin pyrolysis for hydrocarbon production using Ni@HZSM-5-γ-Al_2O_3, J. Anal. Appl. Pyrolysis 166 (2022), 105626.
[8] T. Ding, Y. Wu, X. Zhu, G. Lin, X. Hu, H. Sun, Y. Huang, S. Zhang, H. Zhang, Promoted production of phenolic monomers from lignin-first depolymerization of lignocellulose over Ru supported on biochar by N,P-co-doping, ACS Sustain. Chem. Eng. 10 (2022) 2343–2354.
[9] T. Renders, S. Van den Bosch, S.F. Koelewijn, W. Schutyser, B.F. Sels, Lignin-first biomass fractionation: the advent of active stabilisation strategies, Energy Environ. Sci. 10 (2017) 1551–1557.
[10] W. Li, H. Sun, G. Wang, W. Sui, L. Dai, C. Si, Lignin as a green and multifunctional alternative to phenol for resin synthesis, Green Chem. 25 (2023) 2241–2261.
[11] X. Guo, G. Gao, J. Remón, Y. Ma, Z. Jiang, B. Shi, D.C.W. Tsang, Selective hydrogenation of vanillin to vanillyl alcohol over Pd, Pt, and Au catalysts supported on an advanced nitrogen-containing carbon material produced from food waste, Chem. Eng. J. 440 (2022), 135885.
[12] J.L. Santos, P. Mäki-Arvela, J. Wärnå, A. Monzón, M.A. Centeno, D.Y. Murzin, Hydrodeoxygenation of vanillin over noble metal catalyst supported on biochars: part II: catalytic behaviour, Appl. Catal. B 268 (2020), 118425.
[13] Y. Zhang, J. Zhao, G. Fan, L. Yang, F. Li, Robust MOF-derived carbon-supported bimetallic Ni–Co catalysts for aqueous phase hydrodeoxygenation of vanillin, Dalton Trans. 51 (2022) 2238–2249.
[14] S. Alijani, S. Capelli, C. Evangelisti, L. Prati, A. Villa, S. Cattaneo, Influence of carbon support properties in the hydrodeoxygenation of vanillin as lignin model compound, Catal. Today 367 (2021) 220–227.
[15] S. Iravani, R.S. Varma, Greener synthesis of lignin nanoparticles and their applications, Green Chem. 22 (2020) 612–636.
[16] G. Wang, T. Pang, S. Chen, W. Sui, C. Si, Y. Ni, Fabrication of lignin nanospheres by emulsification in a binary γ-valerolactone/glycerol system and their application as a bifunctional reducer and carrier for Pd nanoparticles with enhanced catalytic activity, Green Chem. 22 (2020) 8594–8603.
[17] J. Ge, G. Wang, W. Sui, C. Si, H. Guo, Y. Ni, J. Hu, Highly efficient metal-acid synergetic catalytic fractionation of lignocellulose under mild conditions over lignin-coordinated N-anchoring Co single-atom catalyst, Chem. Eng. J. 462 (2023), 142109.
[18] C.R. China, S.S. Nyandoro, J.J.E. Munissi, M.M. Maguta, M. Meyer, M. Schroepfer, Tanning capacity of Tessmannia burttii extracts: the potential eco-friendly tanning agents for the leather industry, J. Leather Sci. Eng. 3 (2021) 13.
[19] X. Huang, X. Liao, B. Shi, Synthesis of highly active and reusable supported gold nanoparticles and their catalytic applications to 4-nitrophenol reduction, Green Chem. 13 (2011) 2801–2805.
[20] R. Xi, Y. Tang, R.L. Smith, X. Liu, L. Liu, X. Qi, Selective hydrogenation of glucose to sorbitol with tannic acid-based porous carbon sphere supported Ni–Ru bimetallic catalysts, Green Energy Environ. (2022).
[21] Z. Jiang, J. Duan, X. Guo, Y. Ma, C. Wang, B. Shi, Synthesis of Au/lignin–tannin particles and their anticancer application, Green Chem. 23 (2021) 6945–6952.
[22] X. Meng, C. Crestini, H. Ben, N. Hao, Y. Pu, A.J. Ragauskas, D.S. Argyropoulos, Determination of hydroxyl groups in biorefinery resources via quantitative ^{31}P NMR spectroscopy, Nat. Protoc. 14 (2019) 2627–2647.
[23] F. Yao, S. Xu, Z. Jiang, J. Zhao, C. Hu, The inhibition of p-hydroxyphenyl hydroxyl group in residual lignin on enzymatic hydrolysis of cellulose and its underlying mechanism, Bioresour. Technol. 346 (2022), 126585.

[24] J.L. Santos, C. Megías-Sayago, S. Ivanova, M.Á. Centeno, J.A. Odriozola, Structure-sensitivity of formic acid dehydrogenation reaction over additive-free Pd NPs supported on activated carbon, Chem. Eng. J. 420 (2021), 127641.
[25] K. Vanommeslaeghe, E. Hatcher, C. Acharya, S. Kundu, S. Zhong, J. Shim, E. Darian, O. Guvench, P. Lopes, I. Vorobyov, A.D. Mackerell Jr, CHARMM general force field: a force field for drug-like molecules compatible with the CHARMM all-atom additive biological force fields, J. Comput. Chem. 31 (2010) 671–690.
[26] W.L. Jorgensen, J. Chandrasekhar, J.D. Madura, R.W. Impey, M.L. Klein, Comparison of simple potential functions for simulating liquid water, J. Chem. Phys. 79 (1983) 926–935.
[27] C. Adamo, V. Barone, Toward reliable density functional methods without adjustable parameters: the PBE0 model, J. Chem. Phys. 110 (1999) 6158–6170.
[28] R. Krishnan, J.S. Binkley, R. Seeger, J.A. Pople, Self-consistent molecular orbital methods. XX. A basis set for correlated wave functions, J. Chem. Phys. 72 (1980) 650–654.
[29] A.V. Marenich, C.J. Cramer, D.G. Truhlar, Performance of SM6, SM8, and SMD on the SAMPL1 test set for the prediction of small-molecule solvation free energies, J. Phys. Chem. B 113 (2009) 4538–4543.
[30] F. Xiong, Y. Han, S. Wang, G. Li, T. Qin, Y. Chen, F. Chu, Preparation and formation mechanism of size-controlled lignin nanospheres by self-assembly, Ind. Crop. Prod. 100 (2017) 146–152.
[31] F. Xiong, Y. Han, S. Wang, G. Li, T. Qin, Y. Chen, F. Chu, Preparation and formation mechanism of renewable lignin hollow nanospheres with a single hole by self-assembly, ACS Sustain. Chem. Eng. 5 (2017) 2273–2281.
[32] E. Subbotina, T. Rukkijakan, M.D. Marquez-Medina, X. Yu, M. Johnsson, J.S. M. Samec, Oxidative cleavage of C–C bonds in lignin, Nat. Chem. 13 (2021) 1118–1125.
[33] R. Yu, H. Wang, R. Wang, P. Zhao, Y. Chen, G. Liu, X. Liao, Polyphenol modified natural collagen fibrous network towards sustainable and antibacterial microfiltration membrane for efficient water disinfection, Water Res. 218 (2022), 118469.
[34] Z. Zhang, Y. Liu, J. Wang, T. Xie, L. Sun, Z. Li, A chrome-free combination tanning strategy: based on silicic acid and plant tannin, J. Leather Sci. Eng. 3 (2021) 15.
[35] R.K. Das, A. Mizan, F.T. Zohra, S. Ahmed, K.S. Ahmed, H. Hossain, Extraction of a novel tanning agent from indigenous plant bark and its application in leather processing, J. Leather Sci. Eng. 4 (2022) 18.
[36] Z. Huang, Y. Zeng, Q. Sun, W. Zhang, S. Wang, C. Shen, B. Shi, Insights into the mechanism of flavor compound changes in strong flavor baijiu during storage by using the density functional theory and molecular dynamics simulation, Food Chem. 373 (2022), 131522.
[37] Q. Lin, S. Liao, L. Li, W. Li, F. Yue, F. Peng, J. Ren, Solvent effect on xylose conversion under catalyst-free conditions: insights from molecular dynamics simulation and experiments, Green Chem. 22 (2020) 532–539.
[38] X. Kong, C. Liu, M. Lei, F. Gong, Y. Han, Y. Fan, M. Li, R. Xiao, Critical roles of the oxygen-containing functional groups via β-O-4 lignin linkage hydrogenolysis over copper catalysts, ACS Sustain. Chem. Eng. 9 (2021) 10939–10947.
[39] M. Li, X. Wang, G. Gong, Y. Tang, Y. Zhang, J. Guo, X. Liao, B. Shi, Natural polyphenol-based nanoengineering of collagen-constructed hemoperfusion adsorbent for the excretion of heavy metals, J. Hazard. Mater. 428 (2022), 128145.
[40] X. Guo, S. Zhang, X.-q Shan, Adsorption of metal ions on lignin, J. Hazard. Mater. 151 (2008) 134–142.
[41] H.A.M. Bacelo, S.C.R. Santos, C.M.S. Botelho, Tannin-based biosorbents for environmental applications – a review, Chem. Eng. J. 303 (2016) 575–587.
[42] M. Gurung, B.B. Adhikari, S. Alam, H. Kawakita, K. Ohto, K. Inoue, Persimmon tannin-based new sorption material for resource recycling and recovery of precious metals, Chem. Eng. J. 228 (2013) 405–414.
[43] J. Wang, W. Chen, D. Yang, Z. Fang, W. Liu, T. Xiang, X. Qiu, Monodispersed lignin colloidal spheres with tailorable sizes for bio-photonic materials, Small 18 (2022) 2200671.
[44] G. Yun, S. Pan, T.-Y. Wang, J. Guo, J.J. Richardson, F. Caruso, Synthesis of metal nanoparticles in metal-phenolic networks: catalytic and antimicrobial applications of coated textiles, Adv. Healthc. Mater. 7 (2018) 1700934.
[45] J. Liu, L. Wang, F. Okejiri, J. Luo, J. Zhao, P. Zhang, M. Liu, S. Yang, Z. Zhang, W. Song, W. Zhu, J. Liu, Z. Zhao, G. Feng, C. Xu, S. Dai, Deep understanding of strong metal interface confinement: a journey of Pd/FeO_x catalysts, ACS Catal. 10 (2020) 8950–8959.
[46] A.B. Bindwal, P.D. Vaidya, Reaction kinetics of vanillin hydrogenation in aqueous solutions using a Ru/C catalyst, Energy Fuels 28 (2014) 3357–3362.
[47] J.L. Santos, M. Alda-Onggar, V. Fedorov, M. Peurla, K. Eränen, P. Mäki-Arvela, M.Á. Centeno, D.Y. Murzin, Hydrodeoxygenation of vanillin over carbon supported metal catalysts, Appl. Catal. A 561 (2018) 137–149.
[48] Z. Zhu, X. Xing, D. Feng, Z. Li, Y. Tian, D. Yang, Highly sensitive and fast-response hydrogen sensing of WO_3 nanoparticles via palladium reined spillover effect, Nanoscale 13 (2021) 12669–12675.
[49] Y. Xi, Q. Zhang, H. Cheng, Mechanism of hydrogen spillover on WO_3(001) and formation of H_xWO_3 (x = 0.125, 0.25, 0.375, and 0.5, J. Phys. Chem. C 118 (2014) 494–501.
[50] W. Karim, C. Spreafico, A. Kleibert, J. Gobrecht, J. VandeVondele, Y. Ekinci, J. A. van Bokhoven, Catalyst support effects on hydrogen spillover, Nature 541 (2017) 68–71.
[51] R. Prins, Hydrogen spillover. Facts and fiction, Chem. Rev. 112 (2012) 2714–2738.
[52] W. Xu, K.B. Thapa, Q. Ju, Z. Fang, W. Huang, Heterogeneous catalysts based on mesoporous metal–organic frameworks, Coord. Chem. Rev. 373 (2018) 199–232.
[53] D. Shi, L. Arroyo-Ramírez, J.M. Vohs, The use of bimetallics to control the selectivity for the upgrading of lignin-derived oxygenates: reaction of anisole on Pt and PtZn catalysts, J. Catal. 340 (2016) 219–226.